



HAL
open science

Is Urban Heat Island intensity higher during hot spells and heat waves (Dijon, France, 2014-2019)?

Yves Richard, Benjamin Pohl, Mario Rega, Julien Pergaud, Thomas Thévenin, Justin Emery, Julita Dudek, Thibaut Vairet, Sébastien Zito, Carmela Chateau-Smith

► To cite this version:

Yves Richard, Benjamin Pohl, Mario Rega, Julien Pergaud, Thomas Thévenin, et al.. Is Urban Heat Island intensity higher during hot spells and heat waves (Dijon, France, 2014-2019)?. *Urban Climate*, 2021, 35, pp.100747. 10.1016/j.uclim.2020.100747 . hal-03058359

HAL Id: hal-03058359

<https://hal.science/hal-03058359>

Submitted on 4 Apr 2022

HAL is a multi-disciplinary open access archive for the deposit and dissemination of scientific research documents, whether they are published or not. The documents may come from teaching and research institutions in France or abroad, or from public or private research centers.

L'archive ouverte pluridisciplinaire **HAL**, est destinée au dépôt et à la diffusion de documents scientifiques de niveau recherche, publiés ou non, émanant des établissements d'enseignement et de recherche français ou étrangers, des laboratoires publics ou privés.

Is Urban Heat Island intensity higher during hot spells and heat waves (Dijon, France, 2014–2019)?

5 Yves Richard ^{a,*}, Benjamin Pohl ^a, Mario Rega ^a, Julien Pergaud ^a, Thomas Thevenin ^{b,c}, Justin Emery ^d, Julita Dudek ^{a,c}, Thibaut Vairet ^b, Sébastien Zito ^a, Carmela Chateau-Smith ^e

^a *Centre de Recherches de Climatologie, UMR 6282 Biogéosciences, CNRS/Université Bourgogne Franche-Comté, France*

^b *ThéMA CNRS/Université Bourgogne Franche-Comté, France*

^c *MSH Dijon, Université Bourgogne Franche-Comté, France*

10 ^d *AVENUES, EA 7284, Université de Technologie de Compiègne, France*

^e *CPTC, EA4178, Université Bourgogne Franche-Comté, France*

* *yves.richard@u-bourgogne.fr*

ABSTRACT

15

The Urban Heat Island (UHI) phenomenon is frequently associated with heat waves, both in scientific literature and in the media. Health problems and other issues often result from the co-occurrence of these two phenomena. Previous studies have not yet provided sufficient evidence to validate potential links between UHIs and heat waves. The MUSTARDijon network was set up in 2014, in Dijon, France. Its spatial density (60 sensors) and temporal depth (6 summers) provide information about several Hot Spells and Heat Waves (HS&HW), as well as the daily intensity of UHIs. For the period from June to August (the warmer months), no statistical relationship could be established between temperature and UHI intensity. The UHI phenomenon is strong when days are sunny and not very windy; these two conditions are frequently met during HS&HW, but not systematically. By contrast, these conditions can be fulfilled even without high temperatures. Strong UHIs can thus develop outside Hot Spell/Heat Wave (HS/HW) events. These HS&HW are not necessarily in phase with UHIs: maximum UHI intensity tends to occur before the onset or during the first few days of HS&HW. The intensity of the UHI decreases during HS&HW because nocturnal urban temperature generally remains stationary, whereas rural temperature tends to increase at night. The hypothesis proposed is that this increase in rural night temperature during HS&HW could be linked to the decrease in Actual Evapotranspiration (ETA) and soil wetness.

25

30

Keywords: Urban Heat Island intensity, hot spells & heat waves, hot day, medium-sized city, evapotranspiration, soil moisture

35 1. Introduction

In France and all over the world, heat waves are increasing in frequency, intensity, and duration (Meehl, 2004; Shindell, 2007; Ouzeau et al., 2016; Soubeyroux et al., 2016). Over the next few decades, this increase is likely to continue (Schär et al., 2004; Stott et al., 2004; Barriopedro et al., 2011; Suarez-Gutierrez et al., 2020), raising the question of how communities will adapt to climate change (Adger et al., 2013). Heat waves are particularly deadly in cities (Vandentorren et al., 2004; Robine et al.; 2008; Barriopedro et al., 2011), even more so as they are generally associated with air quality degradation (Shaposhnikov et al., 2014; Churkina et al., 2017). The Urban Heat Island (UHI) phenomenon leads to even higher air temperature in cities, particularly at night (Conti et al., 2005; Habeeb et al., 2015; McGregor et al., 2015; Heaviside et al., 2016; Paravantis et al., 2017; Liao et al.,

45

2018). In hot climates, where air-conditioning is used to cool buildings, UHIs also lead to greater energy consumption (Hatvani-Kovacs et al., 2016). During heat waves in France, UHIs are more likely to lead to health problems (Pascal et al., 2018). An index of vulnerability to thermal stress has already been developed for London (Wolf and McGregor, 2013). Further detailed analysis of the relationship
50 between heat waves and UHIs is essential before proposing coherent solutions for these issues (Masson et al., 2013; Lemonsu et al., 2015; Hendel et al., 2016; Rajkovich and Larsen, 2016; Lehoczky et al., 2017; Daniel et al., 2018).

Studies investigating possible correlations between heat waves and UHI intensity are often based on observations (e.g. Schatz and Kucharik, 2015; Ramamurthy et al., 2017; Rogers et al., 2019), but some
55 studies also include climate modeling with WRF (Weather Research and Forecasting; e.g. Li and Bou-Zeid, 2013; Heaviside et al., 2015; Ramamurthy and Bou-Zeid, 2017; Ortiz et al., 2018; He et al., 2020). Several studies have shown that UHI intensity increases during heat waves, in the UK (Tomlinson et al., 2012; Heaviside et al., 2015), in the USA (Li and Bou-Zeid, 2013; Schatz and Kucharik, 2015; Ramamurthy and Bou-Zeid, 2017; Ramamurthy et al., 2017; Ortiz et al., 2018), in
60 China (He et al., 2020), and in Australia (Rogers et al., 2019). The results for one study in the USA showed an increase in UHI intensity during heat waves for larger cities, but observed no change for smaller cities (Ramamurthy and Bou-Zeid, 2017), while other studies found no change in UHI intensity during heat waves for Oklahoma City (Basara et al., 2008; 2010), or for Atlanta (Zhou and Shepherd, 2010). In Perth (Australia), in surprising contrast with results for Adelaide and Melbourne in the same
65 study, observed UHI intensity was lower during heat waves (Rogers et al., 2019). A comparison of cities in the USA shows that daytime UHI intensity is related to differences in heat convection efficiency between urban and rural areas (Zhao et al., 2014). This convection effect depends on the local background climate (wet or dry). Several hypotheses have been proposed to explain the increase in UHI intensity during heat waves: atmospheric stability (Tomlinson et al., 2012), lower wind speed
70 (Li and Bou-Zeid, 2013), anticyclonic summer conditions (Heaviside et al., 2015), and clearer skies (Schatz and Kucharik, 2015). Factors such as evapotranspiration in rural areas (Li and Bou-Zeid, 2013), and impervious urban surfaces (Ortiz et al., 2018) may also play a role in increasing UHI intensity. Higher UHI intensity can be observed in response to heat waves, even more noticeably at night in Beijing (e.g. He et al., 2020).

75 The link between heat waves and UHI intensity remains difficult to assess, and no true consensus on this precise topic has so far emerged from the literature. To establish whether UHIs are stronger during heat waves, the dataset must be spatially coherent, and cover a long enough period for several heat waves to be recorded. These requirements are met in Dijon (northeastern France) by the Measuring Urban Systems Temperature of Air Round Dijon (MUSTARDijon) network (Richard et al. 2018).
80 Almost half the urban European population (44%) lives in medium-sized cities (Giffinger et al., 2007), of a similar size to Dijon. To investigate potential links between UHIs and heat waves, it is important to analyze the characteristics of both phenomena:

- time of day. The UHI phenomenon intensifies at sunset. How does it evolve during the night, and is the pattern different for heat-wave nights?
- 85 - season. The UHI phenomenon is generally stronger in the warmer months. Does it vary during this period? In spring and early summer, Actual Evapotranspiration (ETa) is at a maximum in rural areas, whereas in mid- and late summer, ETa decreases. This decrease is particularly noticeable in cropland, where ETa is lower after the harvest.
- duration of heat waves. In cities, heat can accumulate during longer heat waves because of building
90 thermal inertia, and the increased use of air-conditioning. In rural areas, ETa may decrease due to soil moisture depletion.

How does UHI intensity evolve during a heat wave? The meteorological conditions before the heat wave period may also affect UHI intensity. Rainfall in the previous days could increase ETa, particularly in rural areas, making soil wetness measurements essential (Imran et al., 2018).

95 In this paper, we use the term Hot Spells and Heat Waves (HS&HW) to cover all hot periods that might have a negative impact on human well-being. We focus on the relationship between UHI intensity and the Hot Spell and Heat Wave (HS/HW) events that have occurred in Dijon since the deployment of the MUSTARDijon network in 2014.

100 This study is structured as follows: in the material and methods section, the study area is presented, then the dataset, the time frame (seasonal and diurnal), the thresholds and criteria used to define HS&HW, and the UHI index. In the results and discussion section, UHI values will be assessed in relation to meteorological variables. The temporal relationship between UHI intensity and HS&HW will be analyzed in detail. Assessing the effects of ETa and soil moisture on UHI evolution during HS&HW will then bring to light potential explanations for the results observed.

105

2. Material and methods

2.1. Data

110 Since June 2014, hourly measurements of temperature (3 m above ground level) have been recorded by the MUSTARDijon network (Richard et al., 2018), with a total of 60 sensors since 2016 (Fig. 1). This network was designed to capture meso-scale rather than micro-scale thermal conditions. Observations collected at Dijon-Longvic (DL), a synoptic weather station operated by Météo-France at an airport site (Fig. 1), include air temperature at 2 m above ground level (DLT), raingauge rainfall (RR1), wind speed at 10 m above ground level (FF), sunshine duration measured in minutes rather than hours (SH), and relative air humidity (RH). Other data for raingauge rainfall (RR2), potential evapotranspiration (ET), actual evapotranspiration (ETa), and Soil Wetness Index (SWI) are taken from Safran-Isba-Modcou (SIM) surface data (8 km * 8 km), a Météo-France product combining observations and model outputs (Soubeyroux et al., 2008). The period studied is from June 6, 2014 (deployment of MUSTARDijon) to July 29, 2019 (end of data collection for this study).

120

2.2. Key phases of the UHI day

125 Maximum UHI intensity is recorded during the warmer months, when heat waves also occur. The season analyzed in this study extends from April 1 to September 30, thus including 968 days and nights during the six warm seasons covered by MUSTARDijon (2014–2019). Data for a UHI day are not assessed from 0000 to 2300 UTC, but from 0700 UTC to 0600 UTC, to avoid a night period spanning two calendar dates. Each night is thus associated with the previous day. Three key moments within the UHI day are targeted: 1 / afternoon: maximum temperature (1300–1700 UTC); 2 / evening: when the temperature drops sharply, and UHI intensity increases (1900–2300 UTC); 3 / night: minimum temperature (0000–0400) UTC.

130

2.3 UHI Index: Urban Index minus Rural Index

The appropriate Local Climate Zone (LCZ; Stewart and Oke, 2012) was identified for each of the 60 sensors recording air temperature in the MUSTARDijon network (Richard et al., 2018; Fig. 1). An Urban Index and a Rural Index were built from representative sets of sensors, with almost no missing

135 values. The UHI Index is the difference between the Urban Index and the Rural Index. The
MUSTARDijon network contains a sufficient number of sensors for a robust UHI Index to be
calculated, as was the case for Madison, Wisconsin, USA (Schatz and Kucharik, 2012).

The Urban Index corresponds to LCZ2, in the city center (Fig. 1), as no area of Dijon corresponds to
LCZ1 (Richard et al., 2018). The mean temperature was calculated for the only two sensors that fit the
140 selection criteria (Place de la Libération and rue Chancelier de l'Hôpital, Fig. 1). Suitable candidate
sensors for the Rural Index are located in sparsely built or unbuilt areas, at some distance from the city
center, but at a comparable elevation. As sensors are attached to street lamps, few MUSTARDijon
sensors are located in LCZA–G (Fig. 1). To the west, the plateaus and valley bottoms cause
topographic effects (e.g. nocturnal inversions) that are not integrated into the LCZ typology, thus
145 complicating any interpretation of the results (Suomi, 2014, Ketterer and Matzarakis, 2015, Leconte et
al., 2017, Lee and Oh, 2018). The four sensors retained for the Rural Index are therefore Ahuy (LCZ9)
to the north, Saint-Apollinaire (LCZD/104) and Magny-sur-Tille (LCZ9) to the east, and Perrigny-lès-
Dijon (LCZD/104) to the south (Fig. 1). The mean temperature for these four sensors was then
calculated. The UHI is defined as the difference between the Urban Index and the Rural Index (UHI =
150 Urban – Rural). The DL station was not selected for the Rural Index, as Météo-France equipment is
different from MUSTARDijon sensors.

2.4. Hot Spells and Heat Waves (HS&HW)

To identify HS&HW, two thresholds were applied to DLT. These thresholds, for maximum daily
155 temperature (DLTx), and minimum daily temperature for the following night (DLTn), were set to select
the largest possible sample, which unfortunately remains rather small for statistical analysis.
Thresholds set for DLTx > 32 °C and DLTn > 16 °C identify clearly recognizable hot days. These
values are, however, below the risk prevention thresholds (for Dijon, 34 °C and 19 °C) used to trigger
regional health alerts in France. Another criterion used to define heat waves in France is temporal
160 persistence, with a minimum of three consecutive days. The limit set in this study is two consecutive
days, with a threshold of seven consecutive days for long Hot Spell/Heat Wave (HS/HW) events.

3. Results and discussion

165 The first results investigate the relationship between UHI intensity, temperature, and meteorological
conditions, for the warmest six months (April–September), over a six-year period (2014–2019). All
HS&HW occurring within the study period are thus identified. Further analysis of UHI intensity
focuses on the comparison of long HS/HW events, and then on the first seven days of each long
HS/HW.

170

3.1. UHI intensity, temperature, sunshine duration, and wind speed

Values for UHI intensity and DLT are plotted from June to August, for 2014 to 2019 (Fig. 2).
Correlations between UHI intensity and DLT are –0.04 for afternoon, +0.32 for evening, and +0.09 for
night. Although correlations for evening and night are significant ($P = 0.01$), the values are low, and no
175 significant correlation is observed for afternoon. When the focus is on the 74 hot days (Fig. 2),
correlations between UHI intensity and DLT are –0.11 for afternoon, –0.12 for evening, and –0.30 for
night, but these slightly negative correlations are not significant. This result may seem counter-

intuitive, because hot days and HS&HW are generally associated with sunshine and almost no wind, meteorological conditions that also result in increased UHI intensity.

180 Figure 3 presents data from April to September for 2015 and 2018, two years with long HS/HW events (see Fig. 4). The following observations can be made:

— during the warmer months, the seasonal temperature pattern is clear, with higher values in July and August (Fig. 3a, e), but no such pattern can be identified for UHI intensity (Fig. 3b, f);

185 — in windy conditions (Fig. 3d, h), the temperature may be high, but UHI intensity is low (Fig. 3, black dotted outline);

— when there is little or no sunshine (Fig. 3c, g), the temperature may still be high, but UHI intensity remains low (Fig. 3, black outline).

190 Although no statistical analysis is presented here, this visual comparison of data from April to September shows that strong UHIs can occur on days with sunshine when there is almost no wind. High temperature (Fig. 3a, e) is not always a key condition for higher UHI intensity (Fig. 3, red outline). Synchronicity between hot days and UHI intensity is not systematically observed during the warmer months.

3.2. UHI intensity and long HS&HW

195 All the HS&HW during the study period (2014–2019) occur between June 19 and August 31, with most occurring in July (Fig. 4). Three long HS/HW events (≥ 7 days) are identified in 2015, one in 2018, and two in 2019. Of the 53 days within these HS&HW, 14 are below the maximum daily temperature threshold, with only 3 days below the minimum daily temperature threshold (Tab. 1). The most affected event is HS/HW 3, with 6 days below the maximum daily temperature threshold, 2 days 200 below the minimum daily temperature threshold, missing rainfall data for 3 of the days, low sunshine duration values, and a noticeable rainfall event (10.2 mm). In HS/HW 1 and in HS/HW 6, only one day is slightly below (31.9 °C) the maximum daily temperature threshold, while all values for HS/HW 5 are above the thresholds.

205 Direct comparison between DLT and UHI for each long HS/HW, aligned over a 30-day period, shows that the two phenomena are out of phase, both hourly and daily (Fig. 5). As expected, UHI intensity is highest in the evening and at night, whereas maximum DLT occurs in the afternoon. More surprisingly, maximum UHI intensity tends to occur slightly before the onset of long HS&HW, and is generally limited to the first few days of HS&HW.

210 No clear pattern is discernible in the DLT mean values for the six long HS&HW, aligned (as in Fig. 5) over a 30-day period (Fig. 6a). Mean daily DLT values show substantial variation for the first seven days and for the entire duration of the six long HS&HW,. The maximum daily values for UHI intensity for the six long HS&HW show a similar level of variability (Fig. 6b). There is, however, a general tendency for UHI intensity to diminish over time, more noticeably during HS/HW events 1, 2, and 4, and less clearly for HS/HW events 3, 5, and 6. The negative values suggest a daytime cool 215 island, an interesting result for a compact mid-rise LCZ in a medium-sized city. Daytime cool islands have been observed in Hong-Kong, a compact high-rise high-density city (Yang et al., 2017), and in several other medium-sized cities: Taipei, Taiwan (Chang et al., 2007); Turku, Finland (Suomi and Käyhkö, 2012); Erbil, Iraqi Kurdistan (Rasul et al., 2015); Toulouse, France (Martins, 2016); and Bragança, Portugal (Gonçalves et al., 2018).

220 **3.3. Mean temperature and UHI intensity during the first seven days of long HS&HW**

As the six long HS&HW varied in duration from 7 to 14 days, mean temperature and UHI intensity for all long HS&HW were calculated for each of the first seven days (Fig. 7), for afternoon (Fig. 7a–b), evening (Fig. 7c–d), and night (Fig. 7e–f). Mean temperature for the Rural Index is systematically lower than for the Urban Index, whatever the time of day, for each day of the HS&HW (Fig. 7a, c, and e). Mean temperature is always high in the afternoon, with little difference between the Rural and Urban Indices (Fig. 7a). Mean temperatures are lower during evening and night, with much greater differences between the two indices (Fig. 7c and e). Mean UHI intensity is therefore higher during evening and night (Fig. 7d and f) than in the afternoon (Fig. 7b).

A more detailed analysis of temporal dynamics shows that the Urban Index rises on days 1 and 2, reaches a peak on days 3 to 5, and then falls on days 6 and 7, whatever the time of day (Fig. 7a, c, and e). The same pattern is observed for the Rural Index, but only in the afternoon. The resulting UHI intensity (0.5–1 °C) is stable (Fig. 7b). During the evening and at night (Fig. 7c and e), the Rural Index mean temperature does not fall on days 6 and 7. The resulting UHI intensity is highest on days 1 and 2, slightly lower on days 3 to 5, and lowest on days 6 and 7 (Fig. 7d and f). The standard deviation analysis seems to confirm the reliability of these results, revealing no discernible trend for the six long HS/HW events.

3.4. Relationship between mean values for UHI intensity, soil wetness, and Eta

Further and more detailed exploration is necessary for better understanding of these results. Two unresolved questions are therefore investigated together: the lack of synchronicity between HS&HW and UHI intensity, and the increase in temperature in rural areas together with the decrease in UHI intensity, in the evening and at night, during HS&HW. Maximum UHI intensity tends to occur before the onset of HS&HW, and is generally limited to the first few days, particularly for HS/HW events 1, 2, and 4, and less noticeably for HS/HW events 3, 5, and 6 (Fig. 6). During HS&HW, a gradual increase in evening and night temperatures is observed for the Rural Index, but not for the Urban Index, resulting in lower UHI intensity (Fig. 7).

In rural areas, fewer surfaces are impervious, so soil moisture is higher; greater plant density favors evapotranspiration, leading to lower nocturnal temperatures. Evapotranspiration is less likely to have an impact in cities, because of the greater area covered by impervious surfaces, thus contributing to the limited temporal variation of higher nocturnal temperatures in the Urban Index during HS&HW. The gradual rural warming observed for mean evening and night temperatures during HS&HW could be explained by a decrease in soil wetness and ETa over time.

To test this hypothesis, daily mean and standard deviation (SD) values for soil and weather conditions were calculated for the first seven days of the six long HS&HW (Fig. 8). The data measured at DL include raingauge rainfall (RR1), sunshine duration (SH), wind speed (FF), and relative air humidity (RH). The data produced by SIM analysis include raingauge rainfall (RR2), potential evapotranspiration (ETP), actual evapotranspiration (ETa), and a Soil Wetness Index (SWI). No discernible pattern is observable in weather conditions, for both mean and SD, during the first seven days of the six long HS&HW (Fig. 8). Soil–atmosphere exchanges, however, tend to decrease (Fig. 8g: ETa), probably as a result of low soil moisture (Fig. 8h: SWI). The decrease is more clearly visible in SD than in mean values (Fig. 8g–h), as soil and weather conditions in the days before each of the six long HS&HW are unlikely to be identical.

3.5. Detailed analysis of each long HS/HW

As ET values are a synthesis of several meteorological variables (T, SH, FF, and RH), the

discussion will now focus only on rainfall (RR1 & RR2) and ET, in relation to ETa, SWI, and UHI intensity for each long HS/HW (Fig. 9). Little or no rainfall (RR1) was recorded at DL during five of the six HS&HW (Fig. 9a). Among the uncertainties associated with SIM analysis, rainfall is often the most sensitive. As the results of SIM rainfall analysis (RR2; Fig. 9b) are very similar to the measured RR1 values, the remaining SIM variables may be considered fairly reliable. The SIM analysis covers a much larger area than the DL station, resulting in more frequent rainfall, but lower values. Rainfall data during HS&HW are also sensitive to local summer storms, which could explain the disparity between RR1 and RR2 for HS/HW 3 (Fig. 9a–b). With such low rainfall values, five of the six long HS&HW also show a related decrease in ETa (Fig. 9d) and SWI (Fig. 9e). The ETa values show greater daily variability than the SWI values, as ETa is the result of ET and SWI combined. The daily maximum intensity of UHI (Fig. 9f) over the same period decreases in a similar way to SWI and ETa, with daily variability similar to the ET pattern (Fig. 9c). Some differences in the pattern of UHI intensity are nevertheless observed for HS/HW 3, HS/HW 5, and HS/HW 6. The difference in UHI values between evening and afternoon (Fig. 9g) presents a very similar pattern to the daily maximum UHI intensity (Fig. 9f). The evening increase in UHI intensity is therefore almost equal to the daily maximum UHI intensity, a result coherent with the ETa hypothesis.

The overall pattern for HS/HW 3 is different from that of the other five long HS&HW. It is the only HS/HW with a noticeably high level of rainfall (RR1, Fig. 9a), and even higher values for RR2 (Fig. 9b). In fact, HS/HW 3 includes rainy days that would completely change all physical processes (Table 1). This is not the case with the other HS&HW, with warm anomalies being favored by atmospheric stability and enhanced by soil dryness (Zampieri et al., 2009; Stéfanon et al., 2014; Whan et al., 2015). The SIM values for ETa (Fig. 9d) and SWI (Fig. 9e), which are partly based on RR2 values, show a similar rising pattern, different from the decreasing trend observed for the other long HS/HW events. The high UHI intensity that persists during HS/HW 5 (Fig. 9f) could perhaps be explained by the Rural Index for this period (not shown), where evening and night temperatures show no increase. The ETa (Fig. 9d) and SWI (Fig. 9e) values are high at the onset of HS/HW 5 and remain higher than for the other five HS&HW. In fact, HS/HW 5 is the only long HS/HW to occur entirely in June (Fig. 4), before the end of the harvest, which could contribute to the relatively low nocturnal temperatures observed in the Rural Index. Maximum UHI intensity occurs before maximum DLT (Fig. 6) during HS/HW 6, the hottest event (Fig. 6a), which also has remarkably high ET values (Fig. 9c). The UHI intensity (Fig. 9f) remains high throughout HS/HW 6, despite low values for ETa (Fig. 9d) and SWI (Fig. 9e).

3.6. Spatial analysis of soil wetness and Eta during the first seven days of long HS&HW

Although the SIM data are low resolution (8 km) at the scale of the Dijon administrative area (Dijon Métropole), they provide some spatial information about ETa and SWI (Fig. 10). The daily mean values were calculated for the first seven days of the six long HS&HW. Precise identification of built and unbuilt surfaces within the urban area is not possible at this resolution, but the heterogeneous nature of surfaces in the surrounding areas can be identified, with a marked difference between the wooded areas in the northwest, and the croplands on the plains in the southeast. The ETa values are highest in the northwest, lower in the southeast when the soil is bare, after harvest (which is generally the case during the long HS&HW), and lowest of all in the urban built areas, as expected (Fig. 10a). During the first seven days of the six long HS&HW, mean values decrease for ETa (Fig. 10a) and for SWI (Fig. 10b), throughout the study area. It is not possible to provide a robust quantification of the difference between urban and rural values at this low spatial resolution (8 km), with the limited size of the sample (6 long HS/HW events).

3.7. Perspectives for further studies

315 These preliminary results, from the dense MUSTARDijon network, over a six-year period, provide
sufficient basis for further experiments using high-resolution climate models with an urban canopy
model (e.g. Meso-NH / TEB; Masson, 2000). Sensitivity experiments on soil moisture could provide
information about sensible and latent heat fluxes at the interface between land surface and atmosphere.
Such experiments could help quantify to what extent these fluxes differ (i) between urban and rural
320 areas, (ii) between the early and later stages of HS&HW, and (iii) in the long term, how they could be
perturbed by ongoing climate change. The relative weight of these fluxes, synthesized for instance
through the Bowen ratio, and its variability in space and time, could have considerable impact on the
intensity of local temperature gradients and on UHI intensity. Combining high-resolution climate
models with dense local networks, extended to cover additional parameters (wind speed & direction,
and global radiation), will provide the perennial tools required for long-term investigation of urban
325 climate change.

5. Conclusion

330 In temperate zones, UHI intensity causes societal problems in summer, during HS/HW events. In
general, HS&HW develop in sunny conditions, with little or no wind, which are also the ideal
conditions for an increase in UHI intensity. In Dijon, a medium-sized European city, during the three
warmer months (June to August), there is little correlation between UHI and air temperature, whether
for the entire period, or for those days identified as hot days. There is no synchronicity between UHI
and temperature: UHI intensity is highest before HS&HW onset, or during the first few HS&HW days.
335 During the six long HS&HW identified in this study, the nocturnal gradient between urban and rural
temperatures (used to calculate UHI intensity) decreases, as rural temperatures rise at night. The
decrease in SWI and ETa in rural areas during HS&HW leads to a decrease in surface latent heat
fluxes, closer to urban conditions.

340 The long-term evolution of climate change is a complex problem, with many parameters: summer
temperatures will almost certainly increase, while soil moisture and rainfall will probably decrease. As
dry conditions become more prevalent, UHI intensity, measured as the gradient between nocturnal
urban and rural temperatures, will tend to decrease. Conditions in urban areas will also evolve (with
changes in size, building materials, spatial extent, and surface impermeability). Such changes are
negligible within the six-year period analyzed in this study, but will be more difficult to take into
345 account at a longer time-scale. A systemic approach with climate models can integrate changes in both
climate and urbanization.

Adapting to climate change would not seek to limit UHI intensity, but more generally to reduce
nocturnal temperatures in urban areas and their rural surroundings. Vegetation, soil moisture and ETa
can all contribute to lower temperatures at night. In urban areas, soil moisture and ETa can be raised by
350 increasing vegetation, but irrigation requirements must be taken into account. In temperate zones, many
cities are surrounded by fields of crops that will generally have been harvested before the main
HS&HW period, leaving the soil bare. Forest belts (e.g. the woods northwest of Dijon) and market
gardening could contribute to ecosystemic resilience, with beneficial effects on nocturnal temperatures
within and around the city.

355

Acknowledgments

360 The Agence de l'Environnement et de la Maîtrise de l'Énergie (ADEME) Bourgogne-Franche-Comté (Franck Dumaitre and Patricia Dubois), Dijon Métropole (Oanez Codet-Hache, Marie-Françoise Dodet and Sophie Bientz), Météo-France (Denis Thévenin and Agnès Tamburini), and the Centre de Calcul de l'université de Bourgogne (CCuB) are thanked for financial and technical support.

References

- 365
1. Adger, W.N., Quinn, T., Lorenzoni, I., Murphy, C., Sweeney, J., 2013. Changing social contracts in climate-change adaptation. *Nature Climate Change* 3, 330–333. <https://doi.org/10.1038/nclimate1751>.
 2. Barriopedro, D., Fischer, E.M., Luterbacher, J., Trigo, R.M., Garcia-Herrera, R., 2011. The Hot Summer of 2010: Redrawing the Temperature Record Map of Europe. *Science* 332, 220–224. <https://doi.org/10.1126/science.1201224>.
 - 360 3. Basara, J.B., Hall, P.K., Schroeder, A.J., Illston, B.G., Nemunaitis, K.L., 2008. Diurnal cycle of the Oklahoma City urban heat island. *J. Geophys. Res.* 113, D20109. <https://doi.org/10.1029/2008JD010311>.
 4. Basara, J.B., Basara, H.G., Illston, B.G., Crawford, K.C., 2010. The Impact of the Urban Heat Island during an Intense Heat Wave in Oklahoma City. *Advances in Meteorology* 2010, 1–10. <https://doi.org/10.1155/2010/230365>.
 - 370 5. Chang, C.-R., Li, M.-H., Chang, S.-D., 2007. A preliminary study on the local cool-island intensity of Taipei city parks. *Landscape and Urban Planning* 80, 386–395. <https://doi.org/10.1016/j.landurbplan.2006.09.005>
 6. Churkina, G., Kuik, F., Bonn, B., Lauer, A., Grote, R., Tomiak, K., Butler, T.M., 2017. Effect of VOC Emissions from Vegetation on Air Quality in Berlin during a Heatwave. *Environmental Science & Technology* 51, 6120–6130. <https://doi.org/10.1021/acs.est.6b06514>.
 - 375 7. Conti, S., Meli, P., Minelli, G., Solimini, R., Toccaceli, V., Vichi, M., Beltrano, C., Perini, L., 2005. Epidemiologic study of mortality during the Summer 2003 heat wave in Italy. *Environmental Research* 98, 390–399. <https://doi.org/10.1016/j.envres.2004.10.009>.
 - 380 8. Daniel, M., Lemonsu, A., Vigiúé, V., 2018. Role of watering practices in large-scale urban planning strategies to face the heat-wave risk in future climate. *Urban Climate* 23, 287–308. <https://doi.org/10.1016/j.uclim.2016.11.001>.
 - 385 9. Giffinger, R., Fertner, C., Kramar, H., Meijers, E., others, 2007. City-ranking of European medium-sized cities. *Cent. Reg. Sci. Vienna UT* 1–12.
 10. Gonçalves, A., Ornellas, G., Castro Ribeiro, A., Maia, F., Rocha, A., Feliciano, M., 2018. Urban Cold and Heat Island in the City of Bragança (Portugal). *Climate* 6, 70. <https://doi.org/10.3390/cli6030070>
 11. Habeeb, D., Vargo, J., Stone, B., 2015. Rising heat wave trends in large US cities. *Nat Hazards* 76, 1651–1665. <https://doi.org/10.1007/s11069-014-1563-z>.
 - 390 12. Hatvani-Kovacs, G., Belusko, M., Pockett, J., Boland, J., 2016. Assessment of Heatwave Impacts. *Procedia Engineering* 169, 316–323. <https://doi.org/10.1016/j.proeng.2016.10.039>.
 13. He, X., Wang, J., Feng, J., Yan, Z., Miao, S., Zhang, Y., Xia, J., 2020. Observational and modeling study of interactions between urban heat island and heatwave in Beijing. *Journal of Cleaner Production* 247, 119169. <https://doi.org/10.1016/j.jclepro.2019.119169>.
 - 395 14. Heaviside, C., Cai, X.-M., Vardoulakis, S., 2015. The effects of horizontal advection on the urban heat island in Birmingham and the West Midlands, United Kingdom during a heatwave: Effects of Horizontal Advection on the Birmingham Urban Heat Island. *Q.J.R. Meteorol. Soc.* 141, 1429–1441. <https://doi.org/10.1002/qj.2452>.
 15. Heaviside, C., Vardoulakis, S., Cai, X.-M., 2016. Attribution of mortality to the urban heat island during heatwaves in the West Midlands, UK. *Environ Health* 15, S27. <https://doi.org/10.1186/s12940-016-0100-9>.
 - 400 16. Hendel, M., Gutierrez, P., Colombert, M., Diab, Y., Royon, L., 2016. Measuring the effects of urban heat island mitigation techniques in the field: Application to the case of pavement-watering in Paris. *Urban Climate* 16, 43–58. <https://doi.org/10.1016/j.uclim.2016.02.003/>
 17. Imran, H.M., Kala, J., Ng, A.W.M., Muthukumar, S., 2018. Effectiveness of green and cool roofs in mitigating urban heat island effects during a heatwave event in the city of Melbourne in southeast Australia. *Journal of Cleaner Production* 197, 393–405. <https://doi.org/10.1016/j.jclepro.2018.06.179>.
 - 405 18. Ketterer, C., Matzarakis, A., 2015. Comparison of different methods for the assessment of the urban heat island in Stuttgart, Germany. *International Journal of Biometeorology* 59, 1299–1309. <https://doi.org/10.1007/s00484-014-0940-3>.

- 410 19. Leconte, F., Bouyer, J., Claverie, R., Pétrissans, M., 2017. Analysis of nocturnal air temperature in districts using mobile measurements and a cooling indicator. *Theoretical and Applied Climatology* 130, 365–376. <https://doi.org/10.1007/s00704-016-1886-7>.
20. Lee, D., Oh, K., 2018. Classifying urban climate zones (UCZs) based on statistical analyses. *Urban Climate* 24, 503–516. <https://doi.org/10.1016/j.uclim.2017.06.005>.
- 415 21. Lehoczy, A., Sobrino, J., Skoković, D., Aguilar, E., 2017. The Urban Heat Island Effect in the City of Valencia: A Case Study for Hot Summer Days. *Urban Science* 1, 9. <https://doi.org/10.3390/urbansci1010009>.
22. Lemonsu, A., Vigié, V., Daniel, M., Masson, V., 2015. Vulnerability to heat waves: Impact of urban expansion scenarios on urban heat island and heat stress in Paris (France). *Urban Climate* 14, 586–605. <https://doi.org/10.1016/j.uclim.2015.10.007>.
- 420 23. Li, D., Bou-Zeid, E., 2013. Synergistic Interactions between Urban Heat Islands and Heat Waves: The Impact in Cities Is Larger than the Sum of Its Parts*. *Journal of Applied Meteorology and Climatology* 52, 2051–2064. <https://doi.org/10.1175/JAMC-D-13-02.1>.
24. Liao, W., Liu, X., Li, D., Luo, M., Wang, D., Wang, S., Baldwin, J., Lin, L., Li, X., Feng, K., Hubacek, K., Yang, X., 2018. Stronger Contributions of Urbanization to Heat Wave Trends in Wet Climates. *Geophys. Res. Lett.* 45. <https://doi.org/10.1029/2018GL079679>.
- 425 25. Martins, T.A.L., 2016. Impact of Urban Cool Island measures on outdoor climate and pedestrian comfort: Simulations for a new district of Toulouse, France. *Sustainable Cities and Society* 18.
26. Masson, V., 2000. A Physically-Based Scheme For The Urban Energy Budget In Atmospheric Models. *Boundary-Layer Meteorology* 94, 357–397. <https://doi.org/10.1023/A:1002463829265>.
- 430 27. Masson, V., Lion, Y., Peter, A., Pigeon, G., Buyck, J., Brun, E., 2013. “Grand Paris”: regional landscape change to adapt city to climate warming. *Climatic Change* 117, 769–782. <https://doi.org/10.1007/s10584-012-0579-1>.
28. McGregor, G.R., Bessemoulin, P., Ebi, K.L., Menne, B., World Meteorological Organization, World Health Organization, 2015. Heatwaves and health: guidance on warning-system development..
29. Meehl, G.A., 2004. More Intense, More Frequent, and Longer Lasting Heat Waves in the 21st Century. *Science* 305, 994–997. <https://doi.org/10.1126/science.1098704>.
- 435 30. Ortiz, L.E., Gonzalez, J.E., Wu, W., Schoonen, M., Tongue, J., Bornstein, R., 2018. New York City Impacts on a Regional Heat Wave. *J. Appl. Meteor. Climatol.* 57, 837–851. <https://doi.org/10.1175/JAMC-D-17-0125.1>.
31. Ouzeau, G., Soubeyroux, J.-M., Schneider, M., Vautard, R., Planton, S., 2016. Heat waves analysis over France in present and future climate: Application of a new method on the EURO-CORDEX ensemble. *Climate Services* 4, 1–12. <https://doi.org/10.1016/j.cliser.2016.09.002>.
- 440 32. Paravantis, J., Santamouris, M., Cartalis, C., Efthymiou, C., Kontoulis, N., 2017. Mortality Associated with High Ambient Temperatures, Heatwaves, and the Urban Heat Island in Athens, Greece. *Sustainability* 9, 606. <https://doi.org/10.3390/su9040606>.
33. Pascal, M., Wagner, V., Corso, M., Laaidi, K., Ung, A., Beaudeau, P., 2018. Heat and cold related-mortality in 18 French cities. *Environment International* 121, 189–198. <https://doi.org/10.1016/j.envint.2018.08.049>.
- 445 34. Rajkovich, N., Larsen, L., 2016. A Bicycle-Based Field Measurement System for the Study of Thermal Exposure in Cuyahoga County, Ohio, USA. *International Journal of Environmental Research and Public Health* 13, 159. <https://doi.org/10.3390/ijerph13020159>.
35. Ramamurthy, P., Bou-Zeid, E., 2017. Heatwaves and urban heat islands: A comparative analysis of multiple cities: Heatwaves and Urban Heat Islands. *J. Geophys. Res. Atmos.* 122, 168–178. <https://doi.org/10.1002/2016JD025357>
- 450 36. Ramamurthy, P., González, J., Ortiz, L., Arend, M., Moshary, F., 2017. Impact of heatwave on a megacity: an observational analysis of New York City during July 2016. *Environ. Res. Lett.* 12, 054011. <https://doi.org/10.1088/1748-9326/aa6e59>.
37. Rasul, A., Balzter, H., Smith, C., 2015. Spatial variation of the daytime Surface Urban Cool Island during the dry season in Erbil, Iraqi Kurdistan, from Landsat 8. *Urban Climate* 14, 176–186. <https://doi.org/10.1016/j.uclim.2015.09.001>
- 455 38. Richard, Y., Emery, J., Dudek, J., Pergaud, J., Chateau-Smith, C., Zito, S., Rega, M., Vairet, T., Castel, T., Thévenin, T., Pohl, B., 2018. How relevant are local climate zones and urban climate zones for urban climate research? Dijon (France) as a case study. *Urban Climate* 26, 258–274. <https://doi.org/10.1016/j.uclim.2018.10.002>.
39. Robine, J.-M., Cheung, S.L.K., Le Roy, S., Van Oyen, H., Griffiths, C., Michel, J.-P., Herrmann, F.R., 2008. Death toll exceeded 70,000 in Europe during the summer of 2003. *Comptes Rendus Biologies* 331, 171–178. <https://doi.org/10.1016/j.crv.2007.12.001>.
- 460 40. Rogers, C.D.W., Gallant, A.J.E., Tapper, N.J., 2019. Is the urban heat island exacerbated during heatwaves in southern Australian cities? *Theoretical and Applied Climatology* 137, 441–457. <https://doi.org/10.1007/s00704-018-2599-x>
41. Schär, C., Vidale, P.L., Lüthi, D., Frei, C., Häberli, C., Liniger, M.A., Appenzeller, C., 2004. The role of increasing temperature variability in European summer heatwaves. *Nature* 427, 332–336. <https://doi.org/10.1038/nature02300>.
- 465 42. Schatz, J., Kucharik, C.J., 2015. Urban climate effects on extreme temperatures in Madison, Wisconsin, USA. *Environ. Res. Lett.* 10, 094024. <https://doi.org/10.1088/1748-9326/10/9/094024>.

43. Shaposhnikov, D., Revich, B., Bellander, T., Bedada, G.B., Bottai, M., Kharkova, T., Kvasha, E., Lezina, E., Lind, T., Semutnikova, E., Pershagen, G., 2014. Mortality Related to Air Pollution with the Moscow Heat Wave and Wildfire of 2010: *Epidemiology* 25, 359–364. <https://doi.org/10.1097/EDE.0000000000000090>.
44. Shindell, D., 2007. Estimating the potential for twenty-first century sudden climate change. *Philosophical Transactions of the Royal Society A: Mathematical, Physical and Engineering Sciences* 365, 2675–2694. <https://doi.org/10.1098/rsta.2007.2088>.
45. Soubeyroux, J.-M., Martin, E., Franchisteguy, L., Habets, F., Noilhan, J., Baillon, M., Regimbeau, F., Vidal, J.-P., Lemoigne, P., Morel, S., 2008. Safran-Isba-Modcou (SIM): Un outil pour le suivi hydrométéorologique opérationnel et les études. *Météorologie* 8, 40. <https://doi.org/10.4267/2042/21890>.
46. Soubeyroux, J.-M., Ouzeau, G., Schneider, M., Cabanes, O., Koukoku-Arnaud, R., 2016. Les vagues de chaleur en France: analyse de l'été 2015 et évolutions attendues en climat futur. *Météorologie* 8, 45. <https://doi.org/10.4267/2042/60704>.
47. Stéfanon, M., Drobinski, P., D'Andrea, F., Lebeau-pin-Brossier, C., Bastin, S., 2014. Soil moisture-temperature feedbacks at meso-scale during summer heat waves over Western Europe. *Clim Dyn* 42, 1309–1324. <https://doi.org/10.1007/s00382-013-1794-9>
48. Stewart, I.D., Oke, T.R., 2012. Local Climate Zones for Urban Temperature Studies. *Bulletin of the American Meteorological Society* 93, 1879–1900. <https://doi.org/10.1175/BAMS-D-11-00019.1>.
49. Stott, P.A., Stone, D.A., Allen, M.R., 2004. Human contribution to the European heatwave of 2003. *Nature* 432, 610–614. <https://doi.org/10.1038/nature03089>.
50. Suarez-Gutierrez, L., Müller, W.A., Li, C., Marotzke, J., 2020. Dynamical and thermodynamical drivers of variability in European summer heat extremes. *Clim Dyn*. <https://doi.org/10.1007/s00382-020-05233-2>.
51. Suomi, J., 2014. Characteristics of urban heat island (UHI) in a high-latitude coastal city – a case study of Turku, SW Finland 70.
52. Suomi, J., Käyhkö, J., 2012. The impact of environmental factors on urban temperature variability in the coastal city of Turku, SW Finland. *International Journal of Climatology* 32, 451–463. <https://doi.org/10.1002/joc.2277>
53. Tomlinson, C.J., Chapman, L., Thornes, J.E., Baker, C.J., 2012. Derivation of Birmingham's summer surface urban heat island from MODIS satellite images. *Int. J. Climatol.* 32, 214–224. <https://doi.org/10.1002/joc.2261>.
54. Vandentorren, S., Suzan, F., Medina, S., Pascal, M., Maulpoix, A., Cohen, J.-C., Ledrans, M., 2004. Mortality in 13 French Cities During the August 2003 Heat Wave. *American Journal of Public Health* 94, 1518–1520. <https://doi.org/10.2105/AJPH.94.9.1518>.
55. Whan, K., Zscheischler, J., Orth, R., Shongwe, M., Rahimi, M., Asare, E.O., Seneviratne, S.I., 2015. Impact of soil moisture on extreme maximum temperatures in Europe. *Weather and Climate Extremes* 9, 57–67. <https://doi.org/10.1016/j.wace.2015.05.001>
56. Wolf, T., McGregor, G., 2013. The development of a heat wave vulnerability index for London, United Kingdom. *Weather and Climate Extremes* 1, 59–68. <https://doi.org/10.1016/j.wace.2013.07.004>.
57. Yang, X., Li, Y., Luo, Z., Chan, P.W., 2017. The urban cool island phenomenon in a high-rise high-density city and its mechanisms: The UCI Phenomenon in Hong Kong and its mechanisms. *Int. J. Climatol.* 37, 890–904. <https://doi.org/10.1002/joc.4747>
58. Zampieri, M., D'Andrea, F., Vautard, R., Ciais, P., de Noblet-Ducoudré, N., Yiou, P., 2009. Hot European Summers and the Role of Soil Moisture in the Propagation of Mediterranean Drought. *Journal of Climate* 22, 4747–4758. <https://doi.org/10.1175/2009JCLI2568.1>
59. Zhao, L., Lee, X., Smith, R.B., Oleson, K., 2014. Strong contributions of local background climate to urban heat islands. *Nature* 511, 216–219. <https://doi.org/10.1038/nature134621>. Adger, W.N., Quinn, T., Lorenzoni, I., Murphy, C., Sweeney, J., 2013. Changing social contracts in climate-change adaptation. *Nature Climate Change* 3, 330–333. <https://doi.org/10.1038/nclimate1751>.
60. Zhou, Y., Shepherd, J.M., 2010. Atlanta's urban heat island under extreme heat conditions and potential mitigation strategies. *Nat Hazards* 52, 639–668. <https://doi.org/10.1007/s11069-009-9406-z>.

MUSTARDijon

Measuring Urban Systems Temperature of Air Round Dijon

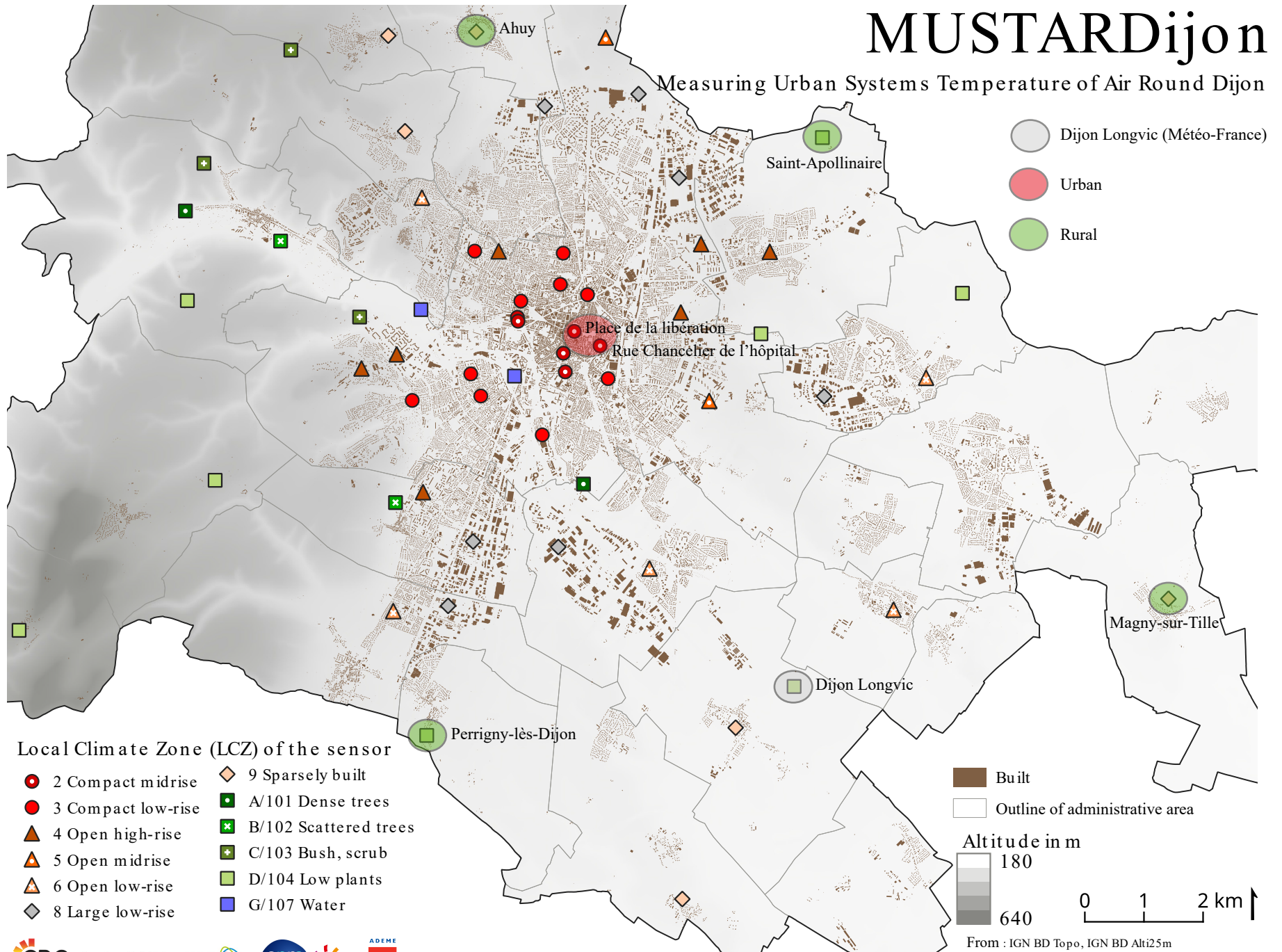


Fig. 1. Map of the study area, showing LCZ, MUSTARDijon sensors, and Dijon-Longvic Météo-France station.

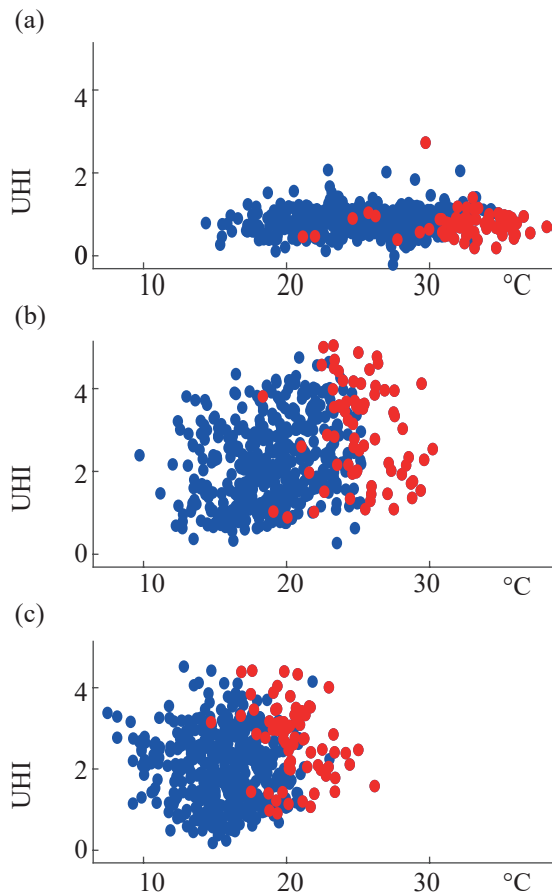


Fig. 2. Scatter plot of UHI intensity & Dijon-Longvic air temperature at 2 m (DLT), in K, June to August 2014-2019.
 (a) Afternoon (1300-1700 UTC) mean.
 (b) Evening (1900-2300 UTC) mean.
 (c) Night (0000-0400 UTC) mean. Red: hot days.
 Blue: days below threshold values ($T_x > 32$ and $T_n > 16^\circ\text{C}$).

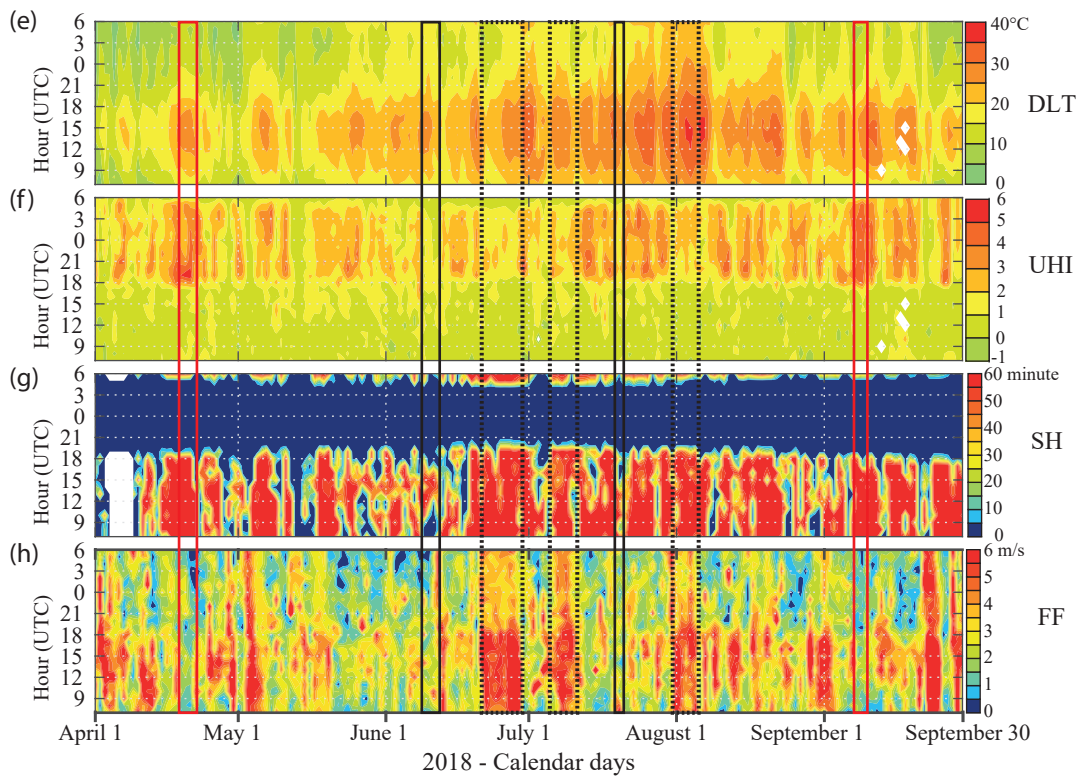
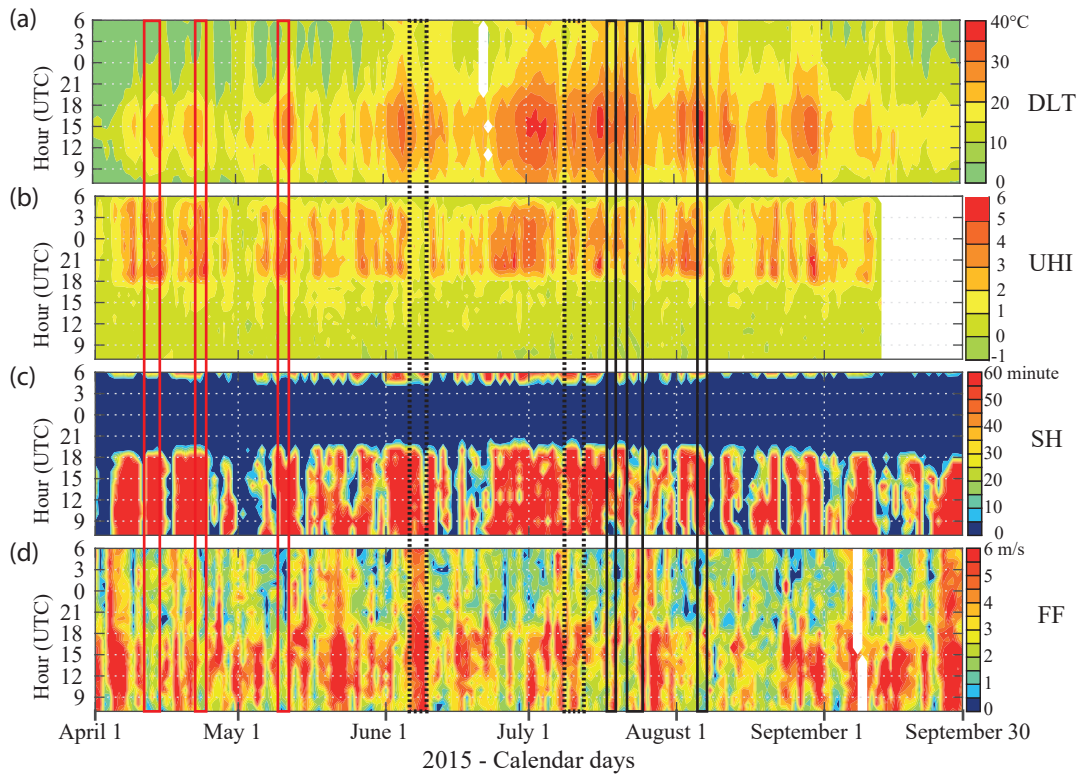
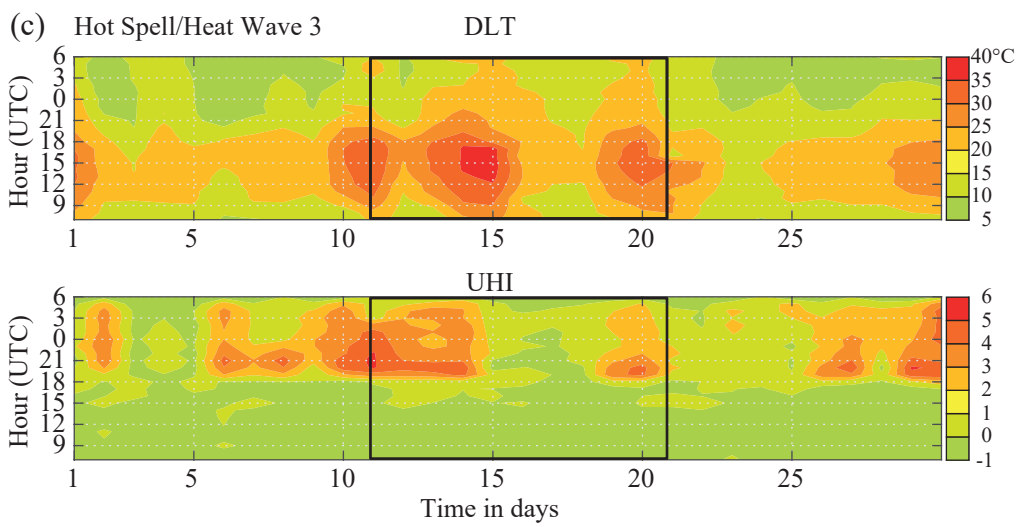
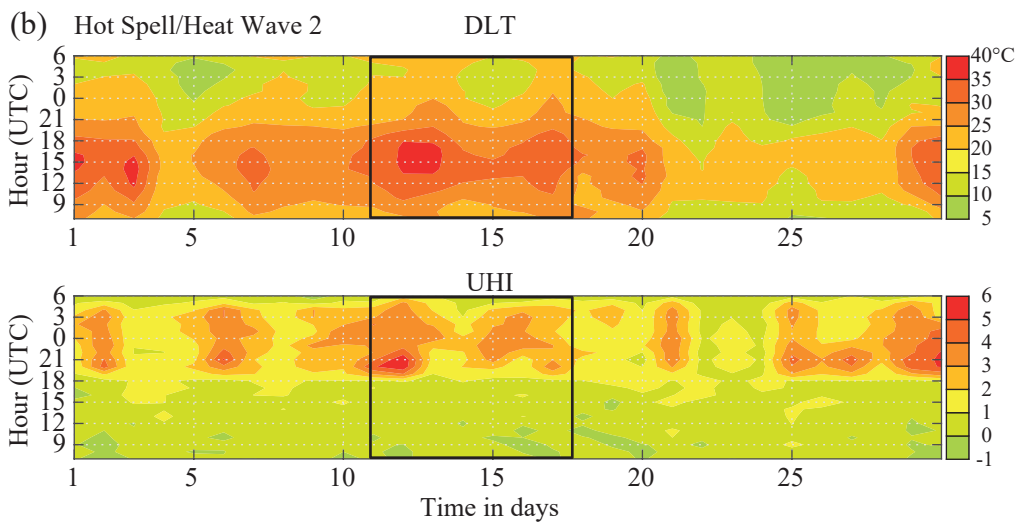
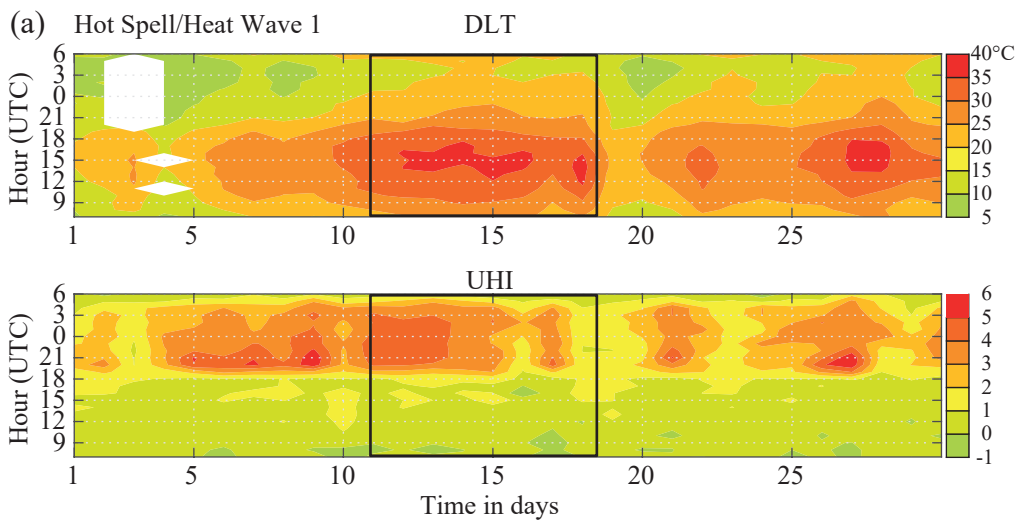


Fig. 3. Meteorological conditions (hourly values)
 April to September: 2015 (a-d) and 2018 (e-h).
 (a) & (e) Dijon-Longvic air temperature at 2 m (DLT) in °C.
 (b) & (f) UHI intensity in K.
 (c) & (g) Sunshine hours (SH) at DL in minute/hour.
 (d) & (h) Wind speed (FF) at DL in m.s-1.
 Red outline: lower T °C, sunny & not very windy, with strong UHI.
 Black outline: higher T °C, not very sunny, without strong UHI.
 Black dotted outline: higher T °C, sunny & windy, without strong UHI.
 N.B. White patches indicate missing data.



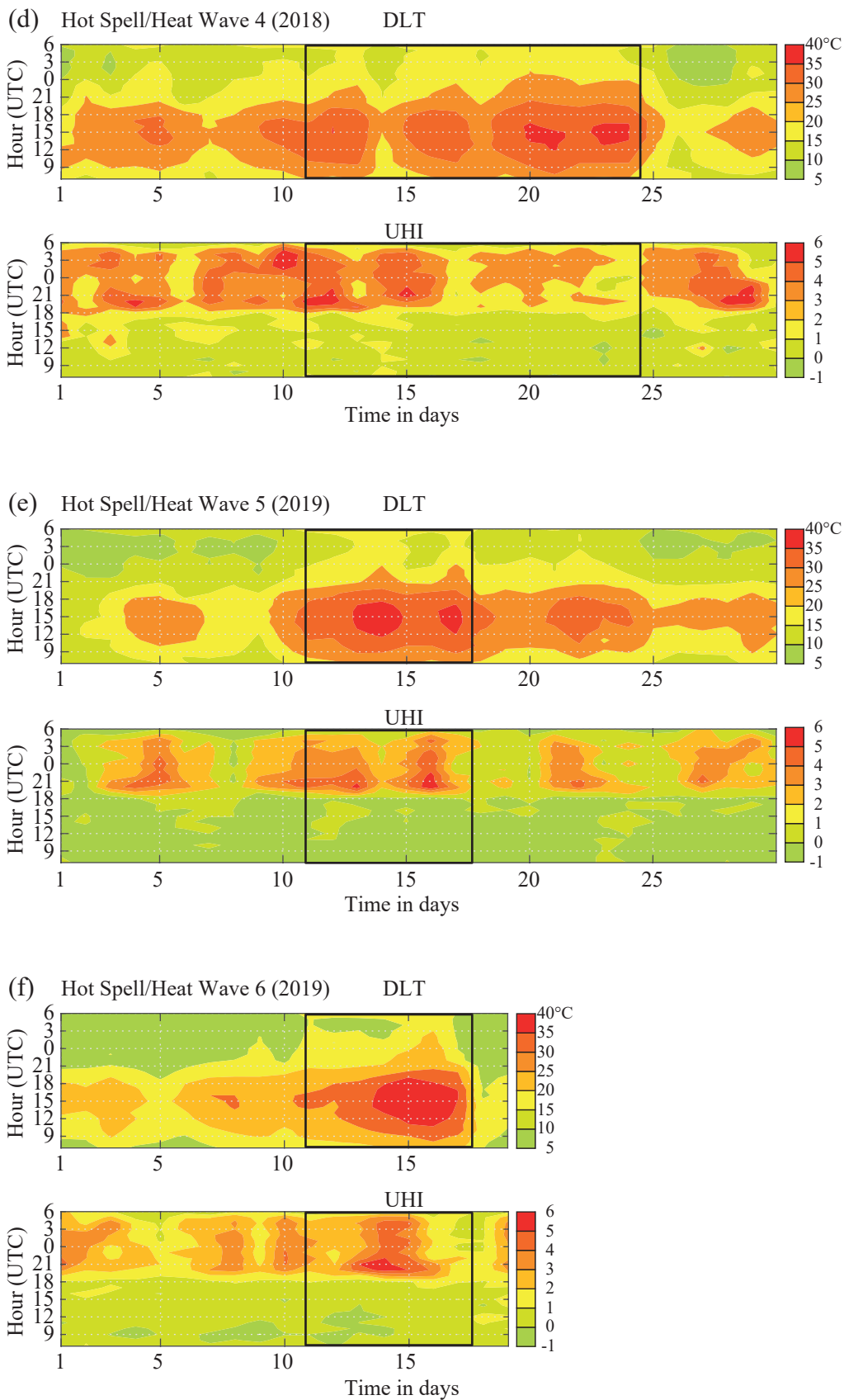


Fig. 5. Comparison of DLT and UHI intensity (hourly values), aligned over a 30-day period.

(a) to (f) Hot Spell/Heat Wave 1 to 6 (see Fig. 2).

DLT air temperature at 2 m at Dijon-Longvic in °C (above).

UHI intensity in K (below). Hot Spell/Heat Wave onset: day 11.

Black outline: total Hot Spell/Heat Wave duration.

NB: White patches indicate missing data.

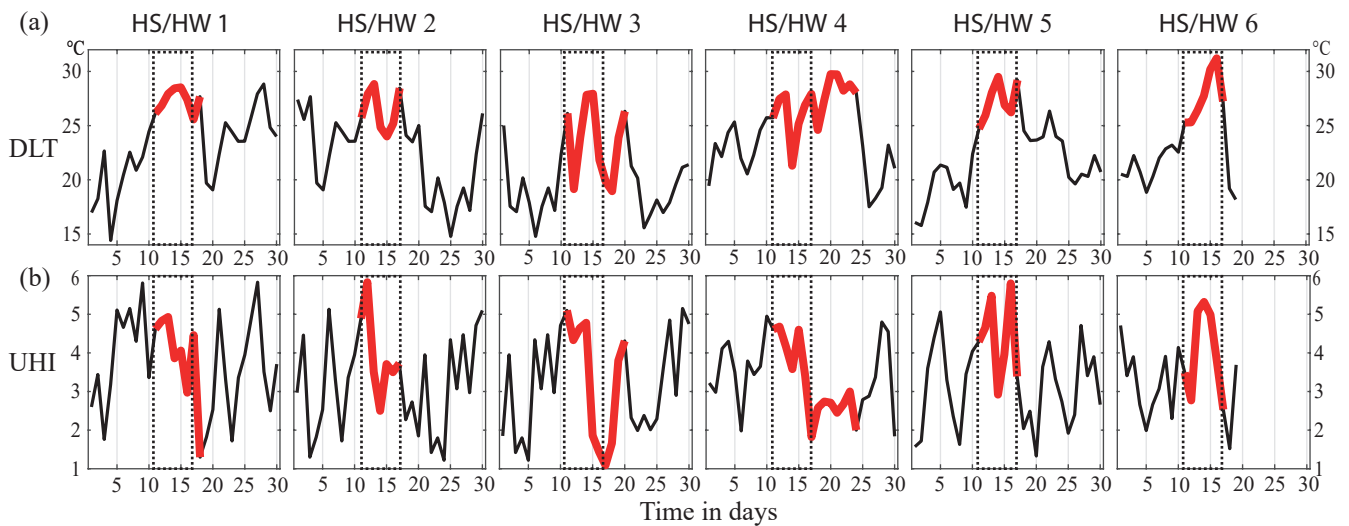


Fig. 6. Evolution of DLT and UHI for each long HS/HW, aligned over a 30-day period.

Each Hot Spell/Heat Wave (HS/HW) is aligned to begin on Day 11.

Red line: values during the HS/HW.

Black line: values before and after the HS/HW.

Black dotted outline: first seven days of the HS/HW.

(a) DLT: Mean daily air temperature at 2 m for Dijon-Longvic in °C.

(b) Maximum daily UHI intensity in K.

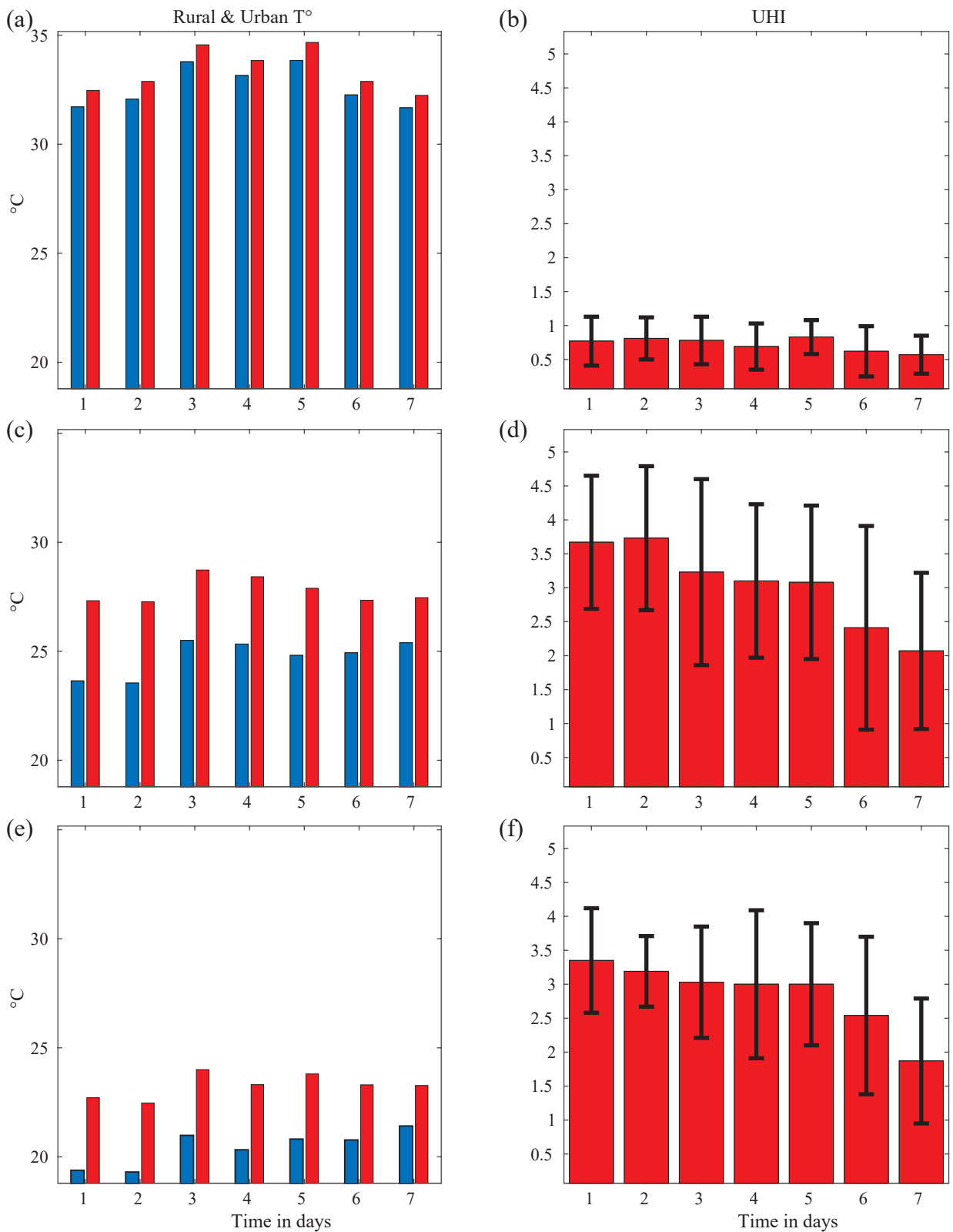


Fig. 7. Mean rural temperature, urban temperature, and UHI intensity for the first seven days during long HS&HW.
 (a) & (b): Afternoon (1300-1700 UTC).
 (c) & (d) Evening (1900-2300 UTC).
 (e) & (f) Night (0000-0400 UTC).
 (a), (c), & (e): T °C (rural in blue, urban in red).
 (b), (d), & (f) UHI intensity in K (mean +/- SD indicated by black error bars).

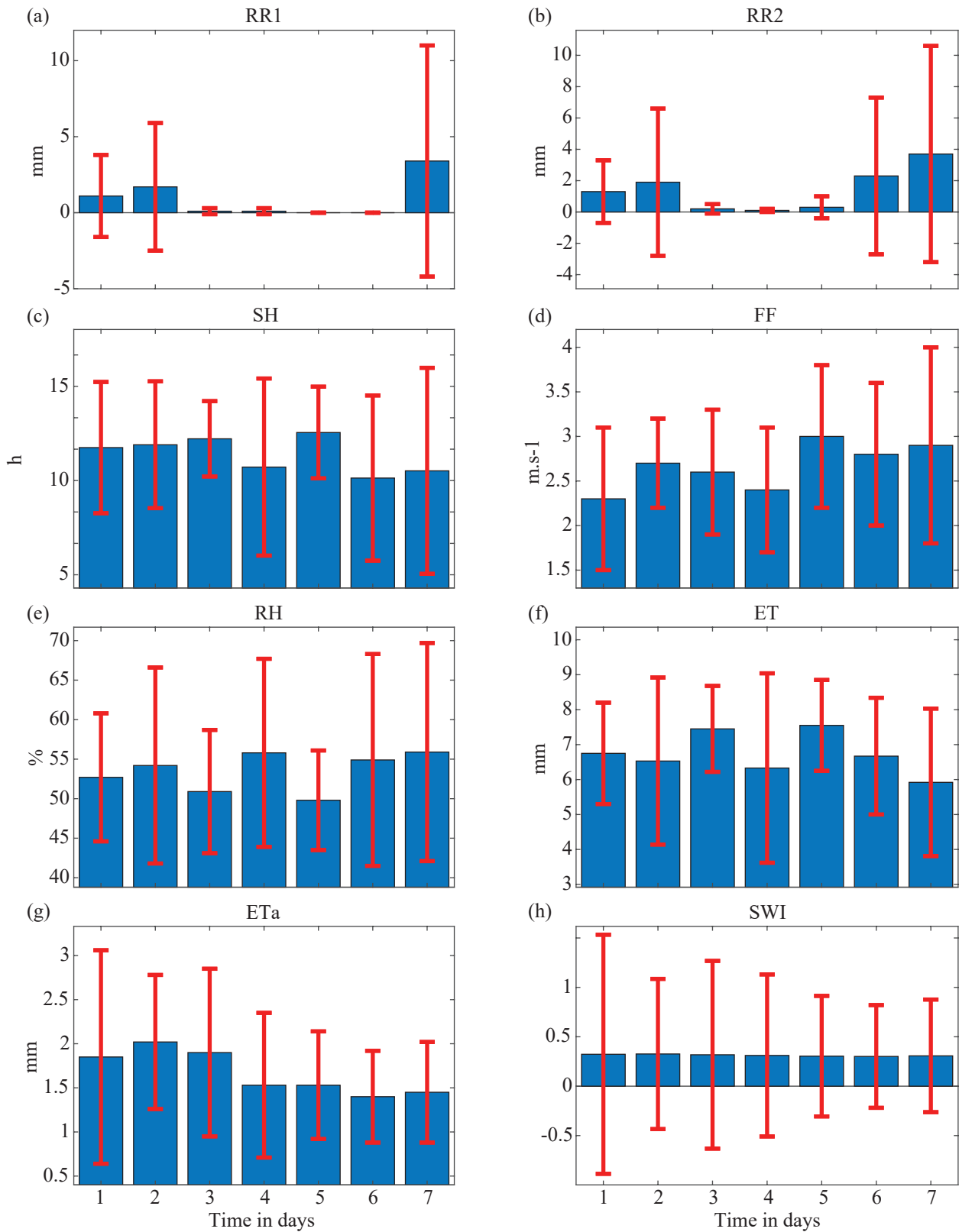


Fig. 8. Mean meteorological and soil conditions for the first seven days during long HS&HW.

(a) RR1: daily rainfall, observed at DL.

(b) RR2: daily rainfall, mean of 4 grid-points analyzed in SIM.

(c) SH: sunshine duration (DL).

(d) FF: wind speed (DL).

(e) RH: relative air humidity (DL).

(f) ET: potential evapotranspiration (SIM).

(g) ETa: actual evapotranspiration (SIM).

(h) SWI: soil wetness index (SIM).

Mean +/- SD indicated by red error bars.

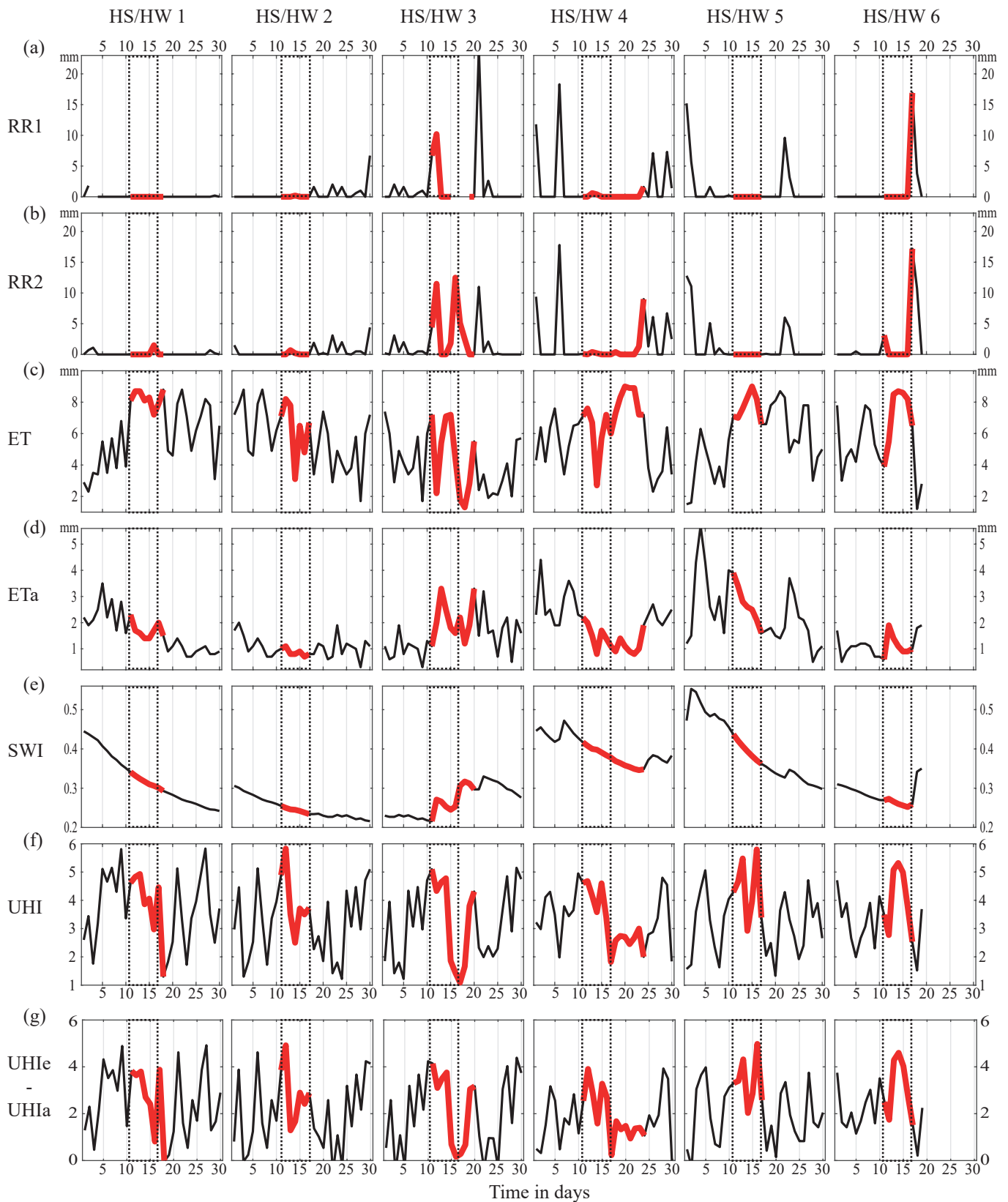


Fig. 9. Meteorological and soil conditions for each long HS/HW, aligned over a 30-day period.

Each Hot Spell/Heat Wave (HS/HW) is aligned to begin on Day 11.

Red line: values during the HS/HW.

Black line: values before and after the HS/HW.

Black dotted outline: first seven days of the HS/HW.

(a) RR1: rainfall observed at Dijon-Longvic.

(b) RR2: rainfall mean of 4 grid-points analyzed in SIM.

(c) ET: potential evapotranspiration (SIM).

(d) ETa: actual evapotranspiration (SIM).

(e) SWI: soil wetness index (SIM).

(f) UHI intensity in K, MUSTARDijon.

(g) UHIe - UHIa: difference in K between UHI evening and UHI afternoon.

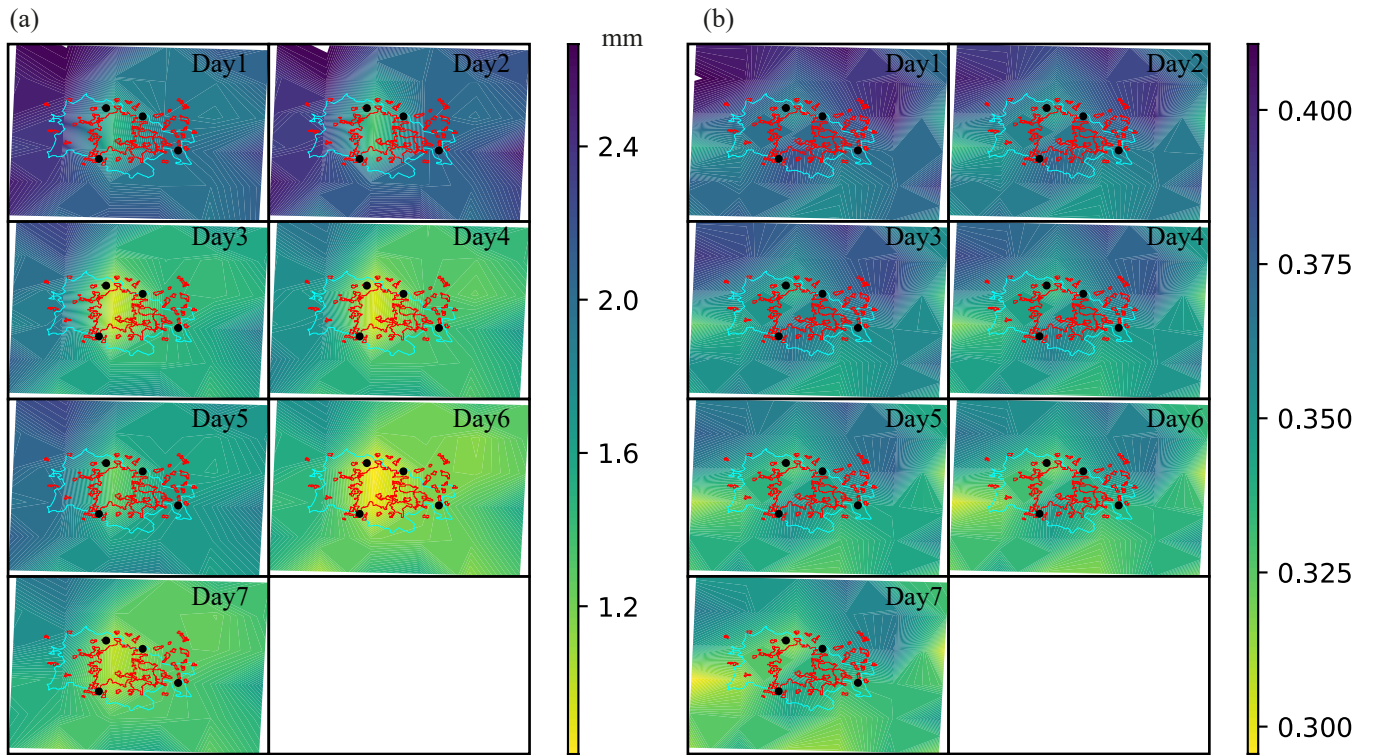


Fig. 10. Mean for ETa and SWI during the first seven days of the six long HS&HW.
 Light blue outline: Dijon administrative area (Dijon Métropole).
 Red outlines: built areas.
 Black dots: grid-points used in Figs. 8 & 9.
 (a) ETa in mm.
 (b) SWI.

Year	Month	Day	HS/HW	DLTn	DLTx	RR1	SH
2015	7	6	1	18,8	31,9	0	875
2015	7	18		19,1	32	0,2	314
2015	7	19	2	16,7	30,9	0	499
2015	7	20		17,6	31,9	0	556
2015	8	4		13,7	26,7	10,2	341
2015	8	5		15,1	31,1	0	720
2015	8	8	3	18,6	24,9	NA	132
2015	8	9		18,2	22,5	NA	7
2015	8	10		16,6	21,7	NA	1
2015	8	11		19,1	29,5	0	572
2018	7	28		15,8	25,9	0,4	253
2018	7	29	4	19,2	30,9	0	854
2018	8	1		19,1	29	0	639
2019	7	21	6	19	31,9	0	641

Table 1: Values for below-threshold days within long Hot Spell

HS/HW: Hot Spell/Heat Wave event.

DLT: Dijon-Longvic air temperature at 2 m in °C.

Orange cells: DLTn ≤ 16 °C. Red cells: DLTx ≤ 32 °C.

RR1: Raingauge rainfall at Dijon-Longvic in mm.

SH: Sunshine duration (measured in minutes).